Electric field induced critical points and polarization rotations in relaxor ferroelectrics

Zdravko Kutnjak* and Robert Blinc
Jožef Stefan Institute, P.O. Box 3000, 1001 Ljubljana, Slovenia

Y. Ishibashi
Faculty of Business, Aichi Shukutoku University, Nagakute-cho, Aichi Prefecture 480-1197, Japan
(Received 6 March 2007; revised manuscript received 5 June 2007; published 11 September 2007)

The giant electromechanical response in ferroelectric relaxors such as $Pb(Mg_{1/3}Nb_{2/3})O_3$-$PbTiO_3$ (PMN-PT) is of great importance for a number of ultrasonic and medical applications as well as in telecommunications. On the basis of the dielectric, heat capacity, and piezoelectric investigations on PMN-PT crystals of various PT compositions and bias fields, we have recently shown the existence of a line of critical points for the paraelectric to ferroelectric transformations in the composition-temperature-electric field (x-T-E) phase diagram. Here, we show the piezobehavior in more detail and present a theoretical evaluation of the Widom line and the critical line. This line effectively terminates a surface of first order transitions. Above this line, supercritical evolution has been observed. On approaching the critical point, both the enthalpy cost to induce the intermediate monoclinic states and thus the barrier for polarization rotations decrease significantly. The maximum of the piezoelectric response is not at $E=0$, but at the critical field values. It is shown that the critical fluctuations in the proximity of the critical points are directly responsible for the observed enhancement of the electromechanical response in the PMN-PT system. In view of the large electric field dependence of the dielectric constant near the critical point, these systems may also be important as electric field tunable elements.

DOI: 10.1103/PhysRevB.76.104102 PACS number(s): 77.84.Dy, 77.65.−j, 77.80.Bh

I. INTRODUCTION

Classical relaxors such as $Pb(Mg_{1/3}Nb_{2/3})O_3$ (PMN) are perovskite solid solutions characterized by site and charge disorder.[1,2] They show no symmetry breaking transition on cooling but exhibit broad and strongly frequency dependent peaks in the dielectric and electromechanical responses as well as glassy-type freezing.[1–4] In contrast to dipolar glasses,[5] a ferroelectric phase can be induced in relaxors by applying a sufficiently strong electric field.[6–9] This is due to the fact that relaxors consist of small, randomly oriented polar nanoregions,[10–14] which, in view of their relatively large dipole moments, couple to the electric field more efficiently than individual dipoles in dipolar glasses.

The coupling to the electric field is still enhanced if the disorder is reduced by changing the composition, e.g., by adding ferroelectric $PbTiO_3$ (PT) to PMN.[15] The PMN_{1-x}-PT_x system is for $x>0.05$ at low temperatures ferroelectric and rhombohedral up to some specific PT content.[15] At still higher PT concentrations, it undergoes a morphotropic phase transition[16,17] and becomes tetragonal. A giant piezoelectric response is observed near this transition. At higher temperatures, the system becomes paraelectric and cubic for all PT concentrations.

The PMN-PT system exhibits a number of different phases. Pure PMN exhibits in addition to the electric field induced ferroelectric state ($E>E_C$) also an ergodic relaxor state at high and a nonergodic relaxor state at low temperatures ($E<E_C$). For sufficiently high PT concentrations, ferroelectric tetragonal (T), rhombohedral (R), monoclinic (M), and orthorhombic (O) phases occur at low and a paraelectric cubic (C) phase at high temperatures. The spontaneous polarization directions are [001] in the tetragonal ($P4mm$) phase, [111] in the rhombohedral ($R3m$) phase, and [110] in the orthorhombic ($mm2$) phase. There are possibly three different monoclinic phases (M_A, M_B, and M_C)[17–20] between the rhombohedral and tetragonal phases (Fig. 1).

The phase transition between the R and T ferroelectric phases observed by many authors[1,2,11,16,17] becomes degenerate near the morphotropic phase boundary. Schmidt and co-workers[21,22] concluded that the R-T phase transition occurs as a rotation of the polarization through M phases. The piezoelectric effect is due to the coupling between the strain and the polarization. When the polarization is along the cube diagonal, the lattice strain is small, but when the polarization is along the cube axis, the lattice strain is large, resulting in a large piezoelectric effect.

The combinations of stress and electric field are particularly effective to drive the system through the phase transformations.[12,23,24]

Cohen and co-workers[23,24] have studied the polarization rotation mechanism under electric field using first principles calculations. The polarization rotation mechanism has been directly verified by x-ray and polarized light microscopy studies.[17–20,22,25]

It has recently been shown[26] that by applying a sufficiently strong electric field $E \geqslant E_C$, the first order paraelectric to ferroelectric phase transitions in the PMP-PT system terminate in a line of critical points (CL) of the liquid-vapor type above which supercritical behavior is observed. On approaching the critical line ($E \rightarrow E_{CL}$), the piezoelectric coefficients as well as the static dielectric constant and the heat capacity always exhibit maximum values. The electric field necessary for polarization rotations[26] and the energy barriers involved significantly decrease on $E \rightarrow E_{CL}$, thus revealing a new driving mechanism for the giant electromechanical response of relaxors.

Very recently, a study of the phase diagram of PMN for electric bias fields applied along [111], [110], and [100] was

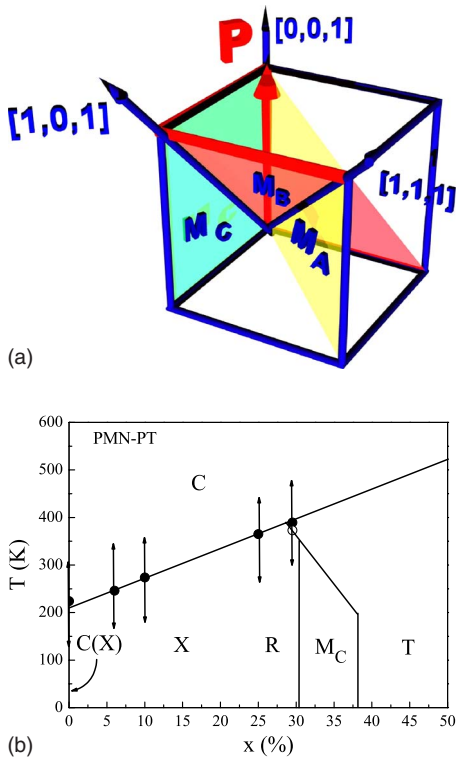

FIG. 1. (Color online) (a) The polarization vector rotates from the $[001]_C$ direction in the tetragonal ($P4mm$) phase to the $[111]_C$ direction in the rhombohedral ($R3m$) phase via the $[110]_C$ direction in the orthorhombic ($mm2$) phase. The polarization vector is within the $(010)_C$, $(\bar{1}01)_C$, and $(1\bar{1}0)_C$ planes in the monoclinic M_C, M_B, and M_A phases, respectively. (b) The composition-temperature (x-T) phase diagram of the PMN-PT system. Double arrows show the compositions measured in this study.

published by Zhao *et al.*[27] Whereas they confirmed the existence of the critical point[27] when the bias field was applied along [111], they did not observe a critical point in the [110] and [100] directions up to the highest applied field of 7.5 kV/cm. In contrast, we here definitely show the existence of critical points for the bias field along [110] in PMN-PT. It should also be noted that all electric field induced transitions occur in PMN at much higher fields than in the PMN-PT system.

The macroscopic symmetry of the PMN-PT system has been studied by optical microscopy in the absence of electric biasing fields by Shuvaeva *et al.*[28]

Here, we relate the observations of the line of critical points in the electric field-temperature (E-T) phase diagram of PMN-PT to the polarization rotation mechanism and the piezoelectric response for fields applied along the [110] and [111] directions. We show that critical points exist not only for [111] but also for [110]. We as well compare the observed critical behavior with the theoretical predictions.

II. EXPERIMENTAL PROCEDURES AND RESULTS

PMN_{1-x}-PT_x single crystals with $x=0$, 0.10, 0.15, 0.25, and 0.295 have been investigated. In all these cases, electric field induced critical points have been found. The necessary electric fields strongly decreased on going from $x=0$ to $x=0.295$. It is this last case on which we shall focus. The electric bias field was applied along the [111] and [110] directions. The field cooled (FC) and zero field cooled quasistatic dielectric (ε) measurements, the measurements of the pyroelectric current, and the polarization (P) determinations were performed by electrometer charge accumulation measurements as described by Levstik *et al.*[29] The phase sequence was determined by polarized light microscopy. The ac dielectric spectroscopy measurements were performed between 1 mHz and 1 GHz. The piezoelectric and elastic coefficients were determined by the resonance response of a platelet[26] poled and excited along its thickness. The radius of the circular platelet was at least ten times larger than the thickness d. High resolution ac and relaxation calorimetry[30,31] in electric fields were used to determine the enthalpy, latent heat, and the critical behavior.

III. THEORY

Let us now discuss the electric field induced critical point in the phase diagram of PMN-PT within the framework of the Landau theory.

The thermodynamic potential density can be in the vicinity of the phase transition expanded in powers of the order parameter P:

$$f = f_0 + \frac{a}{2}P^2 + \frac{b}{4}P^4 + \frac{c}{6}P^6 - PE, \tag{1}$$

where E is the normalized external electric field.

Here, we assumed for sake of simplicity that we deal with a homogeneous medium and a scalar order parameter. We also assume that the polarization and the bias field point in the same direction. The idea is to determine in the simplest possible case the coordinates of the critical point and the evolution of the Widom line in the supercritical region. The treatment of the anisotropic case which is essential for the complete phase diagram close to the morphotropic phase boundaries is nontrivial and will be presented in a subsequent paper. The coefficient a in expression (1) varies with temperature as $a=a_0(T-T_0)/T_0=a_0\tau$ and changes its sign at the phase transition.

For second order phase transitions, one has $b>0$, whereas $b<0$ for first order phase transitions. c is assumed to be always positive, $c>0$.

For second order phase transitions, the critical exponents can be defined for the dielectric susceptibility $\chi(0)$, the order parameter P, and the specific heat at constant pressure C_p as

$$f_{PP}^{-1} = \chi(0) \propto |\tau|^{-\gamma}, \tag{2a}$$

$$P_0(\tau < 0) \propto |\tau|^{\beta}, \tag{2b}$$

$$C_p = -T\left(\frac{\partial^2 f}{\partial T^2}\right)_{P_0} \propto |\tau|^{-\alpha}. \tag{2c}$$

Here, $\partial E/\partial P=(\partial f^2/\partial P^2)_{P_0}=f_{PP}=\chi(0)^{-1}$.

It is well known that the classical values of γ, β, and α in the Landau theory are $\gamma=1$, $\beta=1/2$, and $\alpha=0$. For $b=0$, a tricritical point exists, which separates the line of second order transitions from the line of first order transitions; here, $\beta=1/4$ and $\alpha=1/2$.

Let us now look for the critical point where the line of first order phase transitions terminates. Above the critical point, the anomalies in the response functions become rounded and noncritical, with $\alpha<0$. The difference between the two phases disappears in analogy to the liquid-vapor transition in water.

For a first order ($b<0$) phase transition for $E=0$, the $(f-f_0)$ versus P surface has two minima at $P\neq 0$ in addition to the one at $P=0$. The two additional minima move downward with decreasing T and reach the line $f-f_0=0$ at a positive τ value, i.e., for $T_C>T_0$. For $T<T_C$ these minima have $f-f_0<0$ so that a discontinuous (first order) transition takes place from $P=0$ into one of the two minima with $P\neq 0$. The first order transition takes place when $f-f_0=0$. Solving these equations, we find the transition temperature for $E=0$ as

$$a_C = \frac{3}{16}\frac{b^2}{c}. \tag{3}$$

The temperature (a) dependence of the order parameter for different applied electric fields and the relation between E and P are obtained from

$$\frac{\partial f}{\partial P} = aP + bP^3 + cP^5 - E = 0, \quad b<0, \tag{4a}$$

$$E = aP + bP^3 + cP^5. \tag{4b}$$

The discontinuity in the temperature dependence of the order parameter P is maximal for $E=0$ and vanishes for (a_{CE},E_{CE}), i.e., at the critical point. Let us now determine the T and E coordinates of this point (Fig. 2).

Taking the derivative of expression (4a) with respect to a, we obtain

$$(a + 3bP^2 + 5cP^4)\frac{\partial P}{\partial a} + P = 0. \tag{5}$$

At the transition point, $\partial P/\partial a$ diverges so that

$$(a + 3bP^2 + 5cP^4) = 0. \tag{6}$$

At (a_{CE},E_{CE}), Eq. (6) has a double root so that $9b^2-20ca_{CE}=0$. We thus find the coordinates of the critical point as

$$a_{CE} = \frac{9b^2}{20c}, \tag{7a}$$

$$P_{CE}^2 = \frac{-3b}{10c}, \tag{7b}$$

$$E_{CE} = \frac{6b^2}{25c}\sqrt{\frac{-3b}{10c}}. \tag{7c}$$

Beyond (a_{CE},E_{CE}), the susceptibility χ shows a rounded peak along the Widom line, where $\partial\chi/\partial T=0$ and also

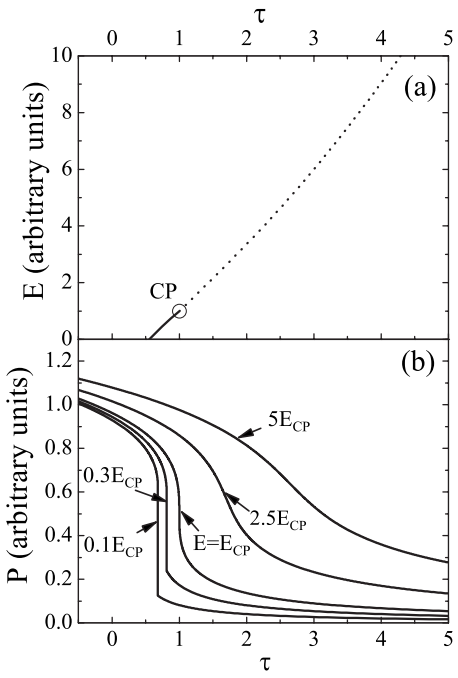

FIG. 2. (a) The schematical E-T phase diagram for the PMN-PT system. The solid line represents a first order transition line. CP stands for the critical point, which terminates a line of first order ferroelectric transitions. The dotted line represents the Widom line, a locus of supercritical anomalies emanating from the critical point typically observed in the supercritical region. (b) The calculated temperature dependence of the order parameter for different bias fields E above and below the critical one (E_{CP}).

$(\partial\chi^{-1}/\partial T)=0$. This is in sharp contrast to the tricritical point beyond which χ diverges at the second order transition line. Beyond (a_{CE},E_{CE}), we thus find with the help of Eq. (4b) the coordinates of the Widom line for a given a as

$$\chi^{-1} = \frac{\partial^2 f}{\partial P^2} = a + 3bP^2 + 5cP^4, \tag{8a}$$

$$\frac{d}{da}(\chi^{-1}) = 1 + (6bP + 20cP^3)\frac{dP}{da} = 0. \tag{8b}$$

These relations thus lead to

$$a - 3bP^2 - 15cP^4 = 0, \tag{9a}$$

$$P_a^{\ 2} = \frac{-b}{10c} + \frac{1}{30c}\sqrt{9b^2 + 60ac}. \tag{9b}$$

Figure 2 shows the schematical E-T phase diagram for the PMN-PT system, based on the above expressions. The theoretical curve agrees rather well with the experimental results.[27] Let us first discuss the [111] case for $PMN_{1-x}PT_x$ with $x=0.295$. For $E=0$, the high temperature phase is cubic and the low T phase rhombohedral. If we apply a bias field along [111], the symmetry including the field is rhombohedral both at low and high temperatures.

Therefore, the two phases can merge at high fields without a boundary, i.e., there exists a critical point.

For the [110] case, the situation is similar. According to Lu *et al.*,[32] the high temperature phase is cubic and the low T phase rhombohedral so that critical points exist in agreement with our observations.

If, however, the system would be monoclinic at low temperatures and tetragonal at high temperatures and the field would be applied along [100], there should be some boundary between the two different symmetries. This problem will be treated as already mentioned in a subsequent paper where the anisotropy of the order parameters will be taken into account.

IV. RESULTS AND DISCUSSION

Let us first look into the behavior of pure PMN at $E\|[111]$. It is known that below a certain temperature, a sufficiently strong electric field $E \geq E_C$ can induce a first order transition from a relaxor state to a ferroelectric state.[7–9] At still higher electric fields, a critical point exists, $E=E_{CL}=4$ kV/cm, above which supercritical behavior is found.[27] Here, we wish to relate the critical response of PMN to its piezoelectric response.

The temperature dependence of the quasistatic FC polarization P of a PMN single crystal poled along [111] has been shown in Refs. 27 and 33 for different electric bias fields. The results can now be compared with the calculated temperature dependence of the order parameter for different electric fields above and below the critical one. For a zero field, the system is in a relaxor state with no spontaneous polarization. For small fields, $E<E_C<E_{CL}$, there is a small induced polarization which continuously increases with decreasing temperature. For $E_C<E<E_{CL}$, there is a jump in the polarization at the first order transition from the relaxor to the ferroelectric state. For $E \geq E_{CL}$, the jump disappears and P continuously varies with temperature in the supercritical regime, in agreement with the theoretical predictions. It should be stressed that it is the continuous supercritical evolution along the Widom line (Fig. 3) which distinguishes the critical point from a tricritical point where a line of first order transition meets a line of second order transition. Whereas in the supercritical case the anomalies in the response functions become noncritically smeared out and finally disappear,[34,35] there are sharp critical anomalies at the line of second order transition in the tricritical case.[36] This is demonstrated in Fig. 4 where the T dependences of the dielectric constant of PMN are presented for different bias fields and frequencies.

Figure 5 also shows the temperature dependence of the piezoelectric coefficient d_{31} for different regions on the Widom line. In all cases, the piezoelectric coefficient shows a noncritical maximum at the evolution line (including the Widom line). The data can be described by

$$d_{im} = \sum_{jk} 2\varepsilon_{ij} Q_{mjk} P_k, \tag{10}$$

where Q_{mjk} are the elements of the electrostrictive tensor, P_k are the components of the spontaneous polarization, and ε_{ij} are the elements of the dielectric tensor. The electric field dependence of the thus obtained maximum values of d_{31} shows itself a clear maximum at the critical point $E=E_{CP}$

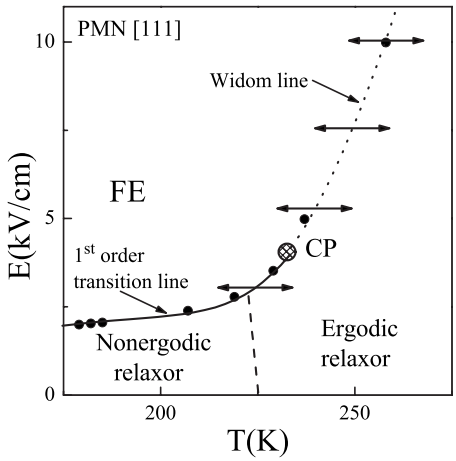

FIG. 3. The electric field-temperature (E-T) phase diagram of a PMN single crystal poled along [111]. The solid line represents a first order transition line. CP stands for the critical point, which terminates a line of first order ferroelectric transitions. The dotted line represents the Widom line, a locus of supercritical anomalies emanating from the critical point typically observed in the supercritical region. Double arrows show the electric bias field values at which the piezoelectric coefficient d_{31} shown in Fig. 4 was measured across the ferroelectric transition and Widom lines.

(Fig. 6). This is mainly a consequence of the fact that response functions such as the dielectric constant ε are at maximum at the critical point.

Let us now turn to the PMN-PT system. The points on the temperature-composition (T-x) phase diagram around which the measurements were performed are shown in Fig. 1(b). For $PMN_{0.75}PT_{0.25}$ and lower concentrations, the critical behavior is similar to that of pure PMN. The discontinuous jump in P at the ferroelectric-paraelectric transition for $E<E_{CL}$ disappears for $E \geq E_{CL}$ and is replaced by a continuous decrease in P with increasing T. The latent heat as well disappears for $E \geq E_{CL}$ so that the values of E_{CL} decrease with increasing χ, i.e., with decreasing disorder.

In the E-T phase diagram, the paraelectric-ferroelectric transition line ends in an isolated critical point above which the difference between the different phases disappears and a continuous supercritical evolution of the response function is observed. The situation gets more complicated with the increasing PT composition toward the morphotropic boundary ($x \approx 0.35$) [Fig. 1(b)]. Already for the composition $x=0.295$ just above the triple point ($x \approx 0.29$), at least four different anomalies have been observed in the temperature dependences of ε, P, and the heat capacity even in the zero field.

The temperature dependence of the dielectric constant ε for a crystal with $x=0.295$ poled along [110] and measured at a bias field of $E=0.03$ kV/cm shows [Fig. 7(a)] at least three additional phases between the R and T ferroelectric states. The different phases have been identified by polarized light microscopy as a monoclinic phase (M_B), an orthorhombic (O) phase, and another monoclinic phase (M_C). The phase sequence $R \rightarrow M_B \rightarrow O \rightarrow M_C \rightarrow T$ is similar to what was found in [111],[33] in agreement with previous findings obtained on [111] and [011] crystals.[32]

The electric field dependence of the transition temperature between these phases is shown in Fig. 7(b). The T-M_C tran-

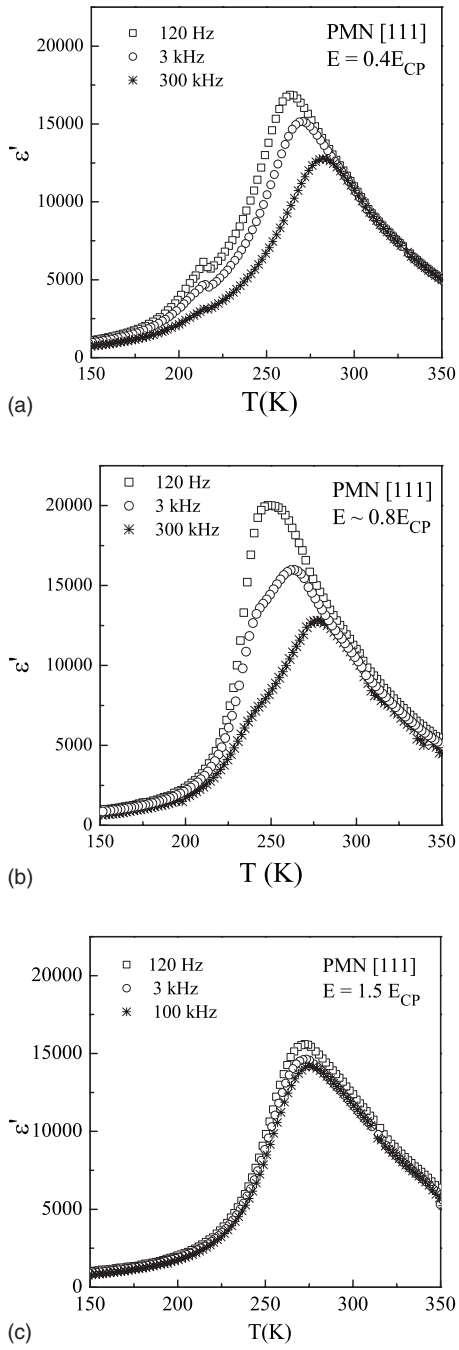

FIG. 4. The temperature dependence of the dielectric constant at different frequencies obtained in a PMN single crystal poled along [111] at three different values of the bias electric field: (a) $0.4E_{CP}$, (b) $0.8E_{CP}$, and (c) $1.5E_{CP}$. Here, E_{CP}=4.0 kV/cm.

sition around 373 K, in particular, is as well critical. As shown by the C_p data [Fig. 9(a)], it is superimposed on the C-T critical transition at 390 K.

The transitions among those phases show up also in the T dependence of the piezoelectric coefficient d_{31}. The corresponding results are shown in Fig. 8 for bias fields E =0.03 kV/cm, E=1.35 kV/cm, and E=2 kV/cm. Note that the our d_{31} data agree well with the low temperature data obtained by Sulc and Pokorny.[37]

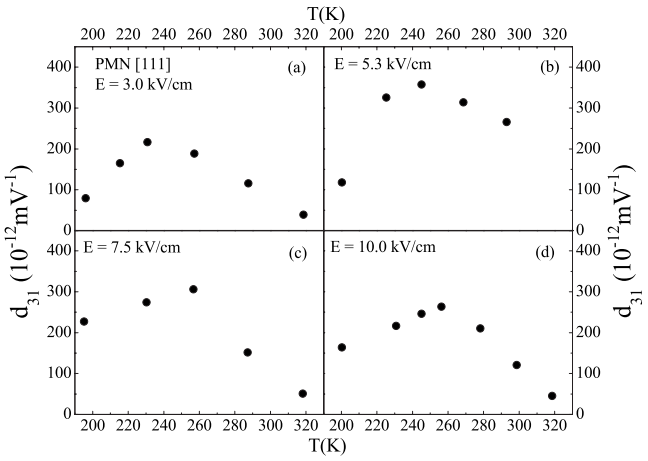

FIG. 5. The temperature dependence of the piezoelectric coefficient d_{31} obtained in a PMN single crystal poled along [111] at four different values of the bias electric field below and above E_{CP} =4.0 kV/cm.

The polarization data for $E\|[111]$ again show[33] that the ferroelectric to paraelectric transition line ends in an isolated critical point E_{CL}=1.3 kV/cm above which supercritical behavior is observed and the difference between the electric field distorted tetragonal and the electric field distorted cubic phases disappears.[33]

According to polarized light microscopy data, the polarization rotates under the applied [111] field at fixed temperature from the T [001] direction into the monoclinic [101] (M_C) plane and then into the orthorhombic [101] direction [Fig. 1(a)]. From there, it goes to the rhombohedral [111] direction via the (101) monoclinic (M_B) plane. The common phase for $E \gg E_{CL}$ should thus be pseudorhombohedral for $E\|[111]$.

The above model is strongly supported by the heat capacity data.[33] These are two critical points: one exists for the C-T and the other for the T-M_C transition. For the T to C

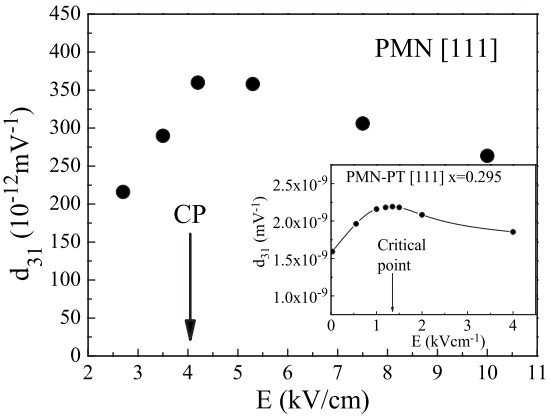

FIG. 6. The electric field dependence of the piezoelectric coefficient d_{31} maximum values along the evolution line of a PMN [111] crystal. The arrow denotes the critical field value E_{CP}. The inset shows the electric field dependence of the piezoelectric coefficient d_{31} along the C-T phase transformation line of a PMN-PT [111] crystal with x=0.295.

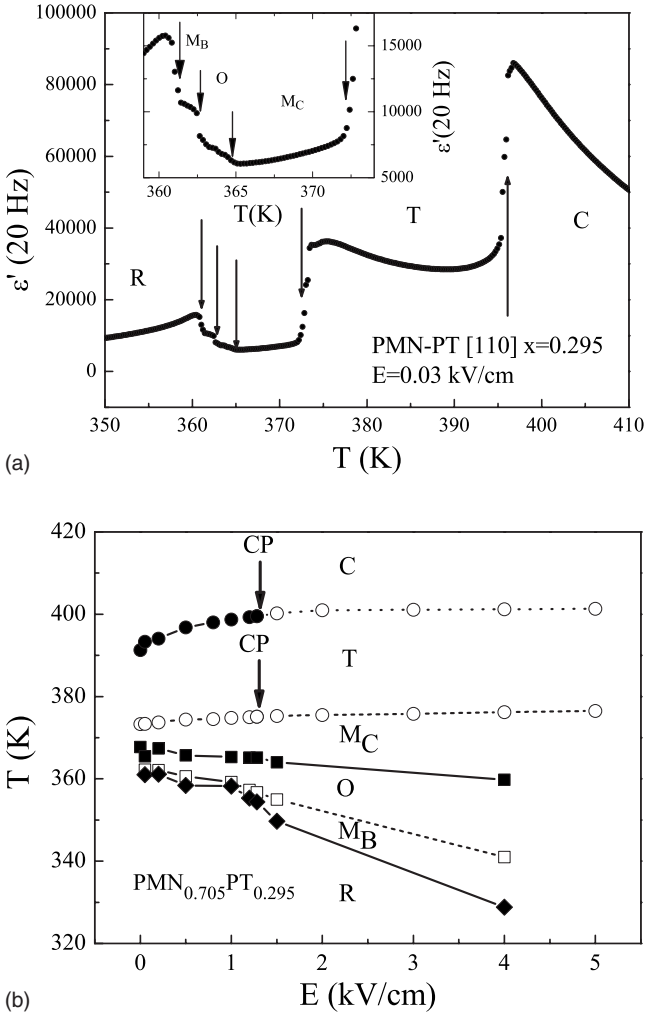

FIG. 7. (a) The temperature dependence of the dielectric constant ε of a PMN-PT crystal poled along the [110] direction with $x=0.295$ and measured at a bias field of $E=0.03$ kV/cm. Note minute steps in the dielectric constant at intermediate monoclinic and orthorhombic phase transitions shown by arrows. (b) The electric field-temperature phase diagram of a PMN-PT crystal with $x=0.295$ poled along the [110] direction and obtained in repeated temperature scans at different constant bias electric fields.

transition at $x=0.295$, the critical point is at $E_{CP}=1.3$ kV/cm. The total enthalpy ΔH exhibits a peak at the electric field corresponding to the critical point[33] [Fig. 9(a)]. The electric field dependence of the enthalpy at the T-M_C transitions is presented in Fig. 9(a) for $E\|[111]$. The inset of Fig. 9(b) shows the electric field dependence of the latent heat L for the T-M_C transition. Again, the latent heat vanishes at $E_{CP}\approx 1.3$ kV/cm. The electric field dependence of the enthalpy for the M_B-R (for $E=0$) transition is shown in Fig. 9(b). The enthalpy changes ΔH for the M_B-O and O-M_C transitions are always below 1 mJ/g. As $P\approx 0.3$ C m^{-2} and $\Delta H\approx E,P$, we find that the necessary electric field for the rotation of the polarization decreases close to the critical point by nearly a factor of 10:

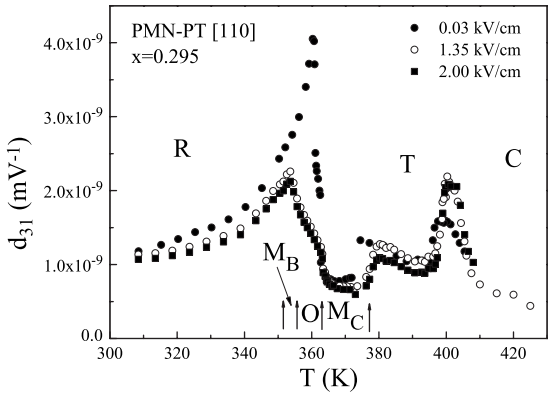

FIG. 8. The temperature dependence of the piezoelectric coefficient d_{31} obtained in a PMN-PT single crystal poled along [110] at three different values of the bias electric field. The phase transition temperatures of intermediate monoclinic and orthorhombic phases obtained at higher bias field values are indicated by arrows.

$$M_C\text{-T:}\quad E_i = 14\ \text{kV/cm} \rightarrow 1.5\ \text{kV/cm}.$$

At the R-M_B transition, the corresponding electric field necessary to induce the polarization rotation is at $E \rightarrow E_{CL}$ reduced to less than 0.4 kV/cm:

$$R\text{-}M_B\text{:}\quad E_i = 2\ \text{kV/cm} \rightarrow 0.4\ \text{kV/cm}.$$

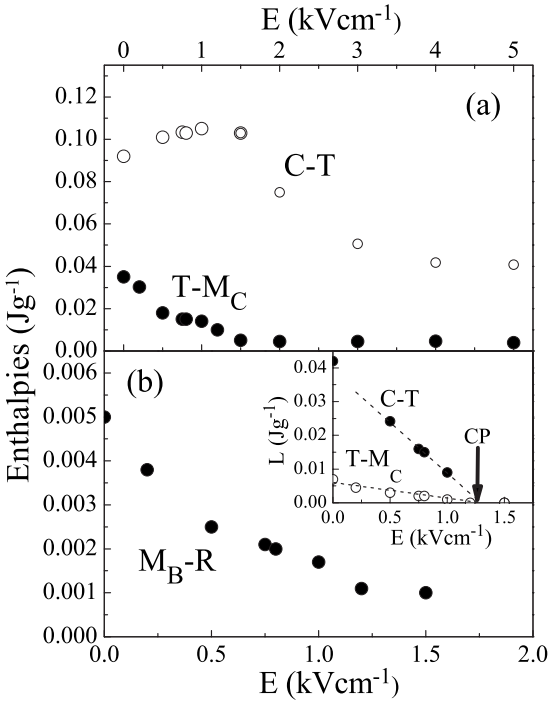

FIG. 9. (a) The total enthalpy ΔH for the C-T transition (open circles) and for the T-M_C transition (solid circles) as a function of the electric bias field applied along the [111] direction. (b) The total enthalpy ΔH for M_B-R transition as a function of the electric bias field. The Arrow indicates the critical value of the electric field. The inset shows the vanishing of the C-T and T-M_C latent heats at the critical field value of $E_{CP}=1.3$ kV/cm.

The electric field dependences of the piezoelectric coefficient d_{31} along the C-T phase transformation line are presented in the inset of Fig. 6. For [111], the maximum value of d_{31} is again at the critical point value E_{CP}. For $E\|[110]$, the situation is more complex, as shown in Fig. 8. Here, it appears as if d_{31} exhibits a maximum value already at the M_B-R phase transition. Fits to the simple power law ansatz

$$d_{31} = At^{-z} + B, \tag{11}$$

with $t=(T-T_C)/T_C$ reveal $z\approx 1.09$, $T_C\sim 376-382$ K for $B\sim(0.27-0.57)\times 10^{-9}$ m V^{-1} [Fig. 10(a)], i.e., the critical dependence of d_{31} observed below the M_B-R phase transition is actually related to the higher temperature T-M_C transition. The critical dependence of d_{31} is just cut off prior to reaching the critical temperature.

This is also confirmed by data sets obtained at different bias electric fields. As shown in Fig. 8, the data sets at different bias fields get slightly suppressed and the cut-off temperature is shifted toward lower temperatures with increasing bias field. If the critical behavior of d_{31} would be related to the M_B-R phase transition, the opposite effect, i.e., enhancement of the data values at given temperature, should be observed. This is due to increasingly lowered M_B-R phase transition temperature with increasing bias field. The decrease of the data values is on the other hand in agreement with the fact that the T-M_C transition temperature is increasing with increasing bias field, thus causing downward rescaling of the d_{31} data at a given fixed temperature.

The above critical behavior of d_{31} is a consequence of the critical dielectric susceptibility related to the nearby critical point fluctuations. As suggested already by Eq. (10), the dielectric constant is the main candidate through which the fluctuations would enter the temperature dependence of d_{31}. As shown in Fig. 10(b), the dielectric constant exhibits in the same temperature range as d_{31} a similar critical behavior, with a similar magnitude of increase (by a factor of ~3.5 when comparing data at 310 K and peak data values), prior to being cut off due to the onset of the M_B-R phase transition. Measurements on unpoled samples indeed show that the dielectric constant below the M_B-R phase transition is actually composed of two contributions. The first contribution represents the critical wing of the C-T transition susceptibility with $T_{C1}\sim 390$ K [see dashed line in Fig. 10(b)]. This contribution does not seem to be affected by the onset of the M_B-R phase transition. The second contribution is related to the low temperature critical wing of the T-M_C phase transition and is superimposed on the first contribution [see the difference between the solid and dashed lines in Fig. 10(b)]. The first contribution is thus effectively playing the role of a temperature dependent background. If this background is subtracted, then $T_{C2}=373$ K is obtained from fits to the simple power law ansatz $\varepsilon' = Ct^{-\gamma}+D$. The thus obtained T_{C2} indeed matches the observed T-M_C phase transition temperature. Here, the classical mean-field value obtained for the $\gamma = 1.0\pm 0.05$ may be due to the fact that the determination is done relatively far from the critical point, i.e., the fits end about 15 K before T_{C2}. This suggests that the critical dependence of d_{31} and its enhancement are a direct consequence of the fluctuations driven by the nearby critical points. This is also confirmed by the electric field dependence [Fig. 10(c)] of the amplitude A in the d_{31} power law ansatz, which exhibits a maximum at the critical field value of $E_{CP}\sim 1.45$ kV/cm (slightly larger E_{CP} in [110]). In fact, the en-

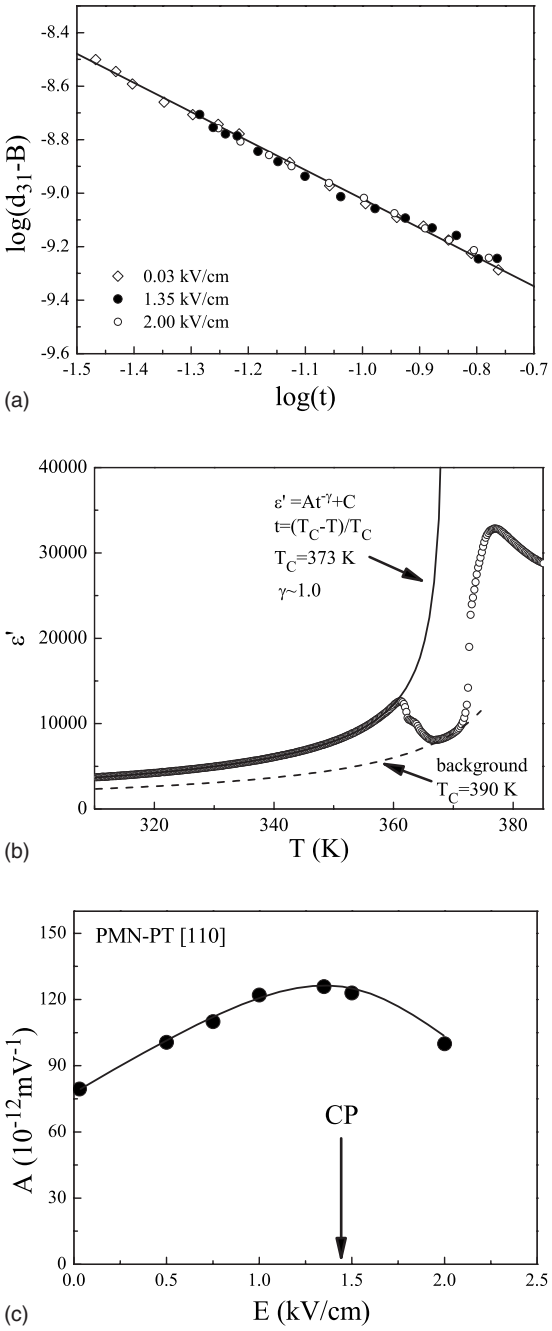

FIG. 10. (a) The temperature behavior of the adjusted piezoelectric coefficient d_{31} obtained on a PMN-PT $x=0.295$ [110] sample. The straight line indicates that the temperature dependence follows a power law behavior. (b) The temperature dependence of the dielectric constant obtained on the same sample at $E=0.03$ kV/cm. The solid line represents a fit to the power law (see the text) after subtraction of the background represented by a dashed line. (c) The electric field dependence of the amplitude A in the d_{31} power ansatz [Eq. (11)], which exhibits a maximum at the critical field value of E_{CP}.

hancement of d_{31} in [110] stems from both C-T and T-M_C critical point fluctuations.

V. CONCLUSIONS

The obtained dielectric and piezoelectric data demonstrate that the electric field induced critical points exist not only for the [111] but also for the [110] direction of the applied bias fields. The existence of the critical points in the E dimension of the T-x-E phase diagram of the PMN-PT system results in a significant enhancement of the piezoelectric coefficients as well as a significant decrease of energy costs and electric fields necessary to induce the R-M_B-O-M_C-T polarization rotations (Fig. 1) producing the giant lattice strains. The system behaves as being effectively semisoft when $E \rightarrow E_{CL}$. The theoretically evaluated E-T critical line agrees qualitatively with the experimental data. The maximum of the piezoelectric response is not achieved at $E=0$, but at $E=E_{CL}$. The electric field induced critical points thus provide a different driving force for the giant electromechanical response. In view of the large electric field dependence of the dielectric constant near the critical point, these systems may also play an important role in electric field tunable optoelectric elements.

ACKNOWLEDGMENTS

This research was supported by the Slovenian Office of Science, Program No. P1-0125 and Project No. J1-9368-0106-06, and the sixth framework EU project "Multiceral," No. NMP3-CT-2006-032616.

*http://www2.ijs.si/~kutnjak
[1] I. E. Cross, Ferroelectrics **76**, 241 (1987).
[2] I. E. Cross, *Ferroelectric Ceramics* (Birkhauser, Berlin, 1993).
[3] A. Levstik, Z. Kutnjak, C. Filipič, and R. Pirc, Phys. Rev. B **57**, 11204 (1998).
[4] Z. Kutnjak, C. Filipič, R. Pirc, A. Levstik, R. Farhi, and M. El Marssi, Phys. Rev. B **59**, 294 (1999).
[5] U. T. Hochli, K. Knorr, and A. Loidl, Adv. Phys. **39**, 405 (1990).
[6] G. Schmidt, H. Arndt, J. von Cieminski, T. Petzsche, H. J. Voigt, and N. N. Krainik, Krist. Tech. **15**, 1415 (1980).
[7] U. Bottger, A. Biermann, and A. Arlt, Ferroelectrics **134**, 253 (1992).
[8] V. Westphal, W. Kleemann, and M. D. Glinchuk, Phys. Rev. Lett. **68**, 847 (1992).
[9] E. V. Colla, E. Y. Koroleva, N. M. Okuneva, and S. B. Vakhrushev, Phys. Rev. Lett. **74**, 1681 (1995).
[10] G. Burns and F. H. Dacol, Solid State Commun. **48**, 853 (1983).
[11] D. Viehland, J. F. Li, S. J. Jang, L. E. Cross, and M. Wuttig, Phys. Rev. B **46**, 8013 (1992).
[12] R. Blinc, J. Dolinšek, A. Gregorovič, B. Zalar, C. Filipič, Z. Kutnjak, A. Levstik, and R. Pirc, Phys. Rev. Lett. **83**, 424 (1999).
[13] Z. Kutnjak, R. Pirc, and R. Blinc, Appl. Phys. Lett. **80**, 3162 (2002).
[14] R. Pirc, R. Blinc, and Z. Kutnjak, Phys. Rev. B **65**, 214101 (2002).
[15] V. E. Colla, N. K. Yushin, and D. Viehland, J. Appl. Phys. **83**, 3298 (1998).
[16] G. Xu, D. Viehland, J. F. Li, P. M. Gehring, and G. Shirane, Phys. Rev. B **68**, 212410 (2003).
[17] F. Bai, N. Wang, J. F. Li, D. Viehland, P. M. Gehring, G. Xu, and G. Shirane, J. Appl. Phys. **96**, 1620 (2004).
[18] D. Viehland and J. Powers, J. Appl. Phys. **89**, 1820 (2001).
[19] M. Davis, D. Damjanović, and N. Setter, J. Appl. Phys. **97**, 064101 (2005).
[20] M. Davis, D. Damjanović, and N. Setter, Phys. Rev. B **73**, 014115 (2006).
[21] C.-S. Tu, I.-C. Shih, V. H. Schmidt, and R. Chien, Appl. Phys. Lett. **83**, 1833 (2003).
[22] R. R. Chien, V. H. Schmidt, C.-S. Tu, L.-W. Hung, and H. Luo, Phys. Rev. B **69**, 172101 (2004).
[23] Z. Wu and R. E. Cohen, Phys. Rev. Lett. **95**, 037601 (2005).
[24] H. Fu and R. E. Cohen, Nature (London) **403**, 281 (2000).
[25] S. Wada, S. Suzuki, T. Noma, T. Suzuki, M. Osada, M. Kakihana, S.-E. Park, L. E. Cross, and T. R. Shrout, Jpn. J. Appl. Phys., Part 1 **38**, 5505 (1999).
[26] V. Bobnar, Z. Kutnjak, and A. Levstik, Jpn. J. Appl. Phys., Part 1 **37**, 5634 (1998).
[27] X. Zhao, W. Qu, X. Tan, A. A. Bokov, and Z. G. Ye, Phys. Rev. B **75**, 104106 (2007).
[28] V. A. Shuvaeva, A. M. Glaser, and D. Zekria, J. Phys.: Condens. Matter **17**, 5709 (2005).
[29] A. Levstik, C. Filipič, Z. Kutnjak, I. Levstik, R. Pirc, B. Tadić, and R. Blinc, Phys. Rev. Lett. **66**, 2368 (1991).
[30] H. Yao, K. Ema, and C. W. Garland, Rev. Sci. Instrum. **69**, 172 (1998).
[31] Z. Kutnjak, S. Kralj, G. Lahajnar, and S. Žumer, Phys. Rev. E **68**, 021705 (2003).
[32] Y. Lu, D.-Y. Jeong, Z.-Y. Cheng, Q. M. Zhang, H.-S. Luo, Z.-W. Yin, and D. Viehland, Appl. Phys. Lett. **78**, 3109 (2001).
[33] Z. Kutnjak, J. Petzelt, and R. Blinc, Nature (London) **441**, 956 (2006).
[34] H. Yao, T. Chan, and C. W. Garland, Phys. Rev. E **51**, 4585 (1995).
[35] Z. Kutnjak, C. W. Garland, C. G. Schatz, P. J. Collings, C. J. Booth, and J. W. Goodby, Phys. Rev. E **53**, 4955 (1996).
[36] K. J. Stine and C. W. Garland, Phys. Rev. A **39**, 3148 (1989).
[37] M. Sulc and M. Pokorny, J. Phys. IV **126**, 77 (2005).